Extended summary

An experimental observation by Nitsche & Straub in *1987* initially showed a fast thermal equilibrium in the absence of convection in supercritical fluids. This phenomenon termed as the 'piston effect' (PE), was predicted theoretically in *1990* by Boukari *et al.*, Onuki *et al.*, and Zappoli *et al.* In the past ten years, most of the attention was devoted to the interaction between the PE and natural convection. Experimental investigations in the Rayleigh-Bénard configuration revealed the development of a convective instability near critical conditions. Direct numerical simulations (DNS) of 2D Navier-Stokes equations contributed to the understanding of the hydrodynamic behavior of such complex flows, where thermal diffusivity vanishes and isothermal compressibility diverges as we approach the critical point. The continuation of previous works led us to extend DNS to fully three-dimensional cases, showing for the first time, to our knowledge, 3D convective structures in a supercritical fluid.

The problem under investigation is shown in figure *1*. A supercritical fluid is enclosed in a cubic shape box, heated from below, and subjected to the earth vertical gravitational field g. Initially, the fluid is at rest, in thermodynamic equilibrium at constant temperature T_i slightly above its critical temperature T_c such that: $T_i = (1+e)T_c$ and $e<<1$. The fluid is stratified in pressure and density, with a mean density equal to its critical value r_c. Numerical simulation starts with the application of a progressive weak heating (DT ~ few mK) to the bottom box wall, while maintaining the upper one at its initial temperature T_i. The governing Navier-Stokes equations are those of a Newtonian, viscous, highly expanding, and heat-conducting van der Waals gas. A $(1+L(T/T_c-1)^{-½})$ law, is used to describe the divergence of the thermal conductivity near the critical point, while heat capacity at constant volume and molecular viscosity are those of a perfect gas. For this study, we consider $T_i-T_c=1K$. The bottom wall temperature is linearly increased (with a slope of *1mK/s*) during one second, then, it is held constant at *1mK* for the rest of the simulation.

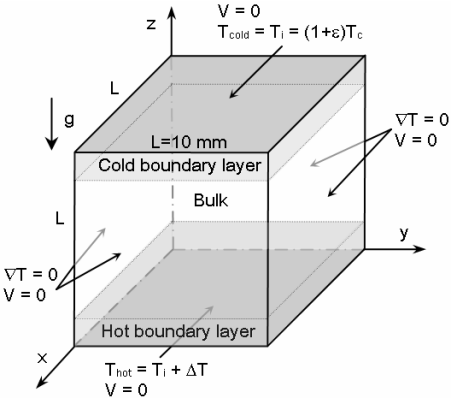

Figure 1. Supercritical fluid in the Rayleigh-Bénard configuration, with no-slip walls and insulated vertical ones.

Governing equations are numerically solved by a fully-implicit finite-volume method on staggered mesh in low Mach number approximation. Space discretization is second order accurate, and unsteady terms are approached with four time levels leading to a third order truncation error in time. For each time step, partial PISO coupling algorithm is performed. Pressure symmetric equation is solved using Conjugate Gradient method while Bi-Conjugate Gradient Stabilized algorithm is used for the other non-symmetric transport equations. A structured, non-uniform, power-law mesh is used, with *120* computational points in each direction (*~1.7* millions degrees of freedom). With a performance of *4.2* Gflops, the code is vectorized and optimally operating on the IDRIS' NEC SX-5 supercomputer. The order of the method was checked using constructed analytical solutions in boussinesq approximation, and the computational code, adapted to a perfect gas flow, was validated by a comparison with a numerical benchmark for natural convection.

Bottom heating induces a wall temperature gradient and the development of a thin thermal boundary layer along the hot wall, a layer in which the density shows large variations due to the hyper-dilatability of near-critical fluids. This boundary layer expands upward, compressing adiabatically the rest of the fluid, and leading to a quick increase of the thermodynamic pressure and to

a fast and homogeneous heating of the cavity bulk by thermo-acoustic effects (PE). As the bulk temperature grows, and since the top wall temperature is maintained at its initial value, a cold boundary layer settles near the top wall. In this PE-dominated phase, the flow is divided into three distinct zones: two thermal boundary layers along the horizontal walls and the cavity bulk. In figure *2*, we represent instantaneous mean temperature fields, *(x,y)* plan mean temperature is plotted as a function of z-coordinate; the profiles at *t=1.2s* and *t=17.9s* show clearly the homogenous increase of the bulk temperature induced by the PE.

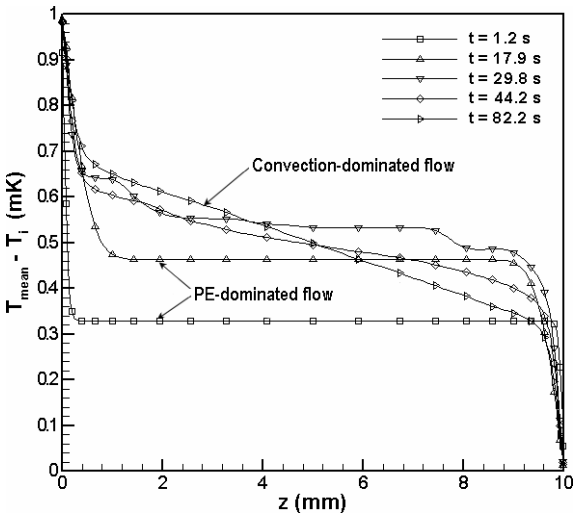

Figure 2. Instantaneous mean temperature in *(x,y)* plan as a function of z-coordinate. In PE-dominated flow, bulk temperature is homogeneously increased by PE; while convective structures speed up the temperature equilibrium in convection-dominated flow.

As long as the flow in the boundary layers is dominated by the diffusion, the thermal boundary layers grow in time at heat diffusion speed. This thermal expansion is hindered by the density stratification of the fluid, leading to a well-known situation ending with a convective instability when the local Rayleigh number exceeds a critical value. Figure *3-a* illustrates convection onset: convective plumes rise from both thermal boundary layers; the space distribution of these structures in *(x,y)* plan seems to match the squared geometric shape. In figure *3-b*, temperature field is subjected to radical changes: on the top wall, a circular distribution of the thermal plumes is observed, while on the bottom wall, some convective structures take vertical fin shapes. In figure *3-c*, these new shapes are more localized on the bottom wall and spread on the insulated walls leaving flat zones where convective plumes rise, are pinched off, and release thermal balls floating upwards, leaving horn-like shafts. The convective improvement of the heat transfer between the isothermal walls and the cavity bulk leads to the faster temperature equilibrium in the whole cavity observed in figure *2* (*t=29.8s, 44.2s, 82.2s*) with the appearance of a bulk slope on the mean temperature profiles.

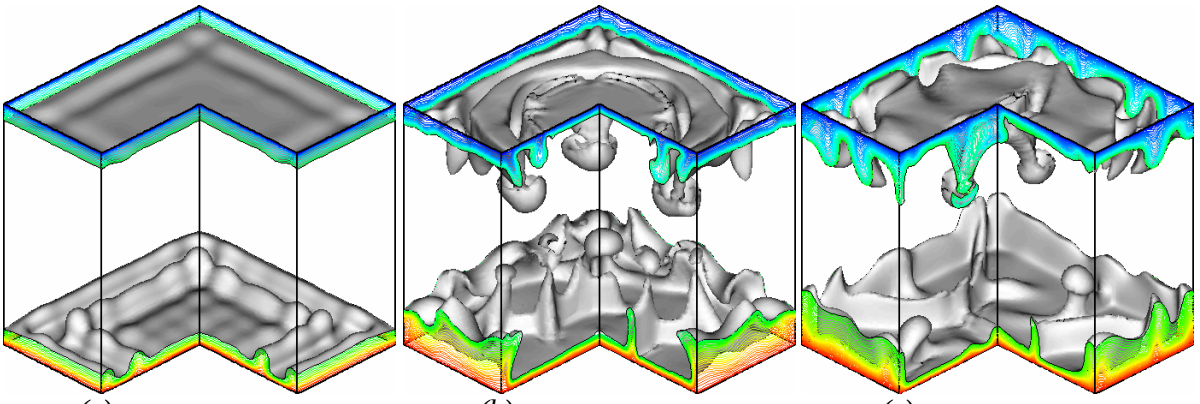

(a) *(b)* *(c)*

Figure 3. Instantaneous temperature fields for *DT=1mK*, exhibiting the three-dimensionality of the flow. From *(a)* to *(c)*, *t = 22.6s*, *36.9s*, *63.1s*, and the shaded isotherms of (T-T_i) in *mK* are respectively: *(0.4,0.6)*, *(0.44,0.6)*, *(0.37,0.65)*